Title
A Comparitive Study of Wavelet Image Coders

Journal
Optical Engineering, 35

Authors
Lu, Jian
Algazi, Ralph
Estes, Robert R.

Publication Date
1996

Peer reviewed

A Comparative Study of Wavelet Image Coders

Jian Lu, V. Ralph Algazi, and Robert R. Estes, Jr.

Center for Image Processing and Integrated Computing (CIPIC)
University of California, Davis, CA 95616
Phone: (916)752-2387 Fax: (916)752-8894
Email: jian@cipic.ucdavis.edu

Revised, July 1996

ABSTRACT

We compare several wavelet-based coders in the encoding of still images. Two image quality metrics are used in our comparative study: a perception-based, quantitative picture quality scale and the conventional distortion measure, peak signal-to-noise ratio. Coders are evaluated in the rate-distortion sense. The effects of different wavelets, quantizers, and encoders are assessed individually. Two representative wavelets, three quantizers, three encoders, and the combinations of these components are compared. Our results provide insight into the design issues of optimizing wavelet coders, as well as a good reference for application developers to choose from an increasingly large family of wavelet coders for their applications.

Subject terms: wavelets, wavelet transform, image coding and compression, image quality, distortion measure.

1 INTRODUCTION

Research in wavelet image coding since the late 1980s has explored various aspects of wavelet image coders.[1–12] Today, this field continues to grow at a rapid pace; reports on new coders and variations of the existing ones are appearing constantly at conferences and in journals. Despite the widespread interest in wavelet coders, there has been no comprehensive and comparative study of the performance of various wavelet coders using a suitable distortion measure. This makes it difficult to consider optimum designs or to choose from an increasingly large family of wavelet coders for specific applications. We were thus motivated to perform a comparative study of wavelet coders.

Our comparative study is confined to still images and is based on rate-distortion measures. A common expectation about wavelet image coders is that they produce subjectively better quality images than the standard Joint Photographic Experts Group (JPEG) coder. This is a well-recognized fact, at least for images encoded at low bit rates. However, an objective evaluation must rely on some quantitative distortion measure. The traditional distortion measure, the mean square error (MSE), has long been recognized as inadequate because of its low correlation with human visual perception. It is particularly inappropriate to use the MSE for evaluating wavelet coders, which are largely motivated by the properties of the human visual system (HVS).[13] We chose to use a perception-based, quantitative distortion measure, called the picture quality scale (PQS), in addition to the commonly used peak signal-to-noise ratio (PSNR) which is based on MSE. The PQS has been developed in the past few years for evaluating the quality of compressed images. It combines various perceived distortions in image coders into a single quantitative measure and it correlates well with the subjective evaluation quantified by a mean opinion score (MOS). In previous research, the JPEG image coder, along with one subband and one wavelet coder, was studied extensively using the PQS.[14]

The design of a wavelet image coder can be divided into three parts: wavelet and related representations, quantization strategies, and error-free encoding techniques. In each part, one has freedom to choose from a pool of candidates and this choice will ultimately affect the coder performance. Therefore, it is necessary to evaluate each choice independently, i.e., with the other parts of the coder fixed. The number of such combinations can be prohibitively large, even after we eliminate some apparently unreasonable choices, so that in this paper, while we review a large number of possible choices for each decision, we present our comparative results using two wavelets, three quantizers, and three encoders on two test images.

The rest of paper is organized as follows: Sec. 2 reviews the family of wavelet image coders by examining different choices of wavelets, quantizers, and encoders; Sec. 3 introduces the PQS, a perceptual distortion measure we adopt in our study in addition to PSNR; Sec. 4 presents experimental results of coder comparisons and some comments; Sec. 5 concludes the paper.

2 FAMILY OF WAVELET IMAGE CODERS

In this section, we review the family of wavelet image coders by examining the options we have for wavelet

representations, quantizers, and encoders. Generally speaking, a wavelet image coder can be made by selecting a wavelet representation, a set of quantizers, and an error-free encoder. However, an arbitrary combination of the three parts does not always make sense in practice. We will point this out as we encounter such situations. Given the abundant literature in wavelet image coding and for the purpose of this paper, we do not intend to give full technical descriptions of wavelet representations, quantizers, and encoders. This section is only a survey of the parts that can be used to build wavelet coders; references are provided for those who desire more details. We realize, however, that our survey can hardly be complete in such a fast developing technical area.

2.1 Wavelet Representations

Wavelet representations differ in their choice of wavelets. We discuss a few general types of wavelets and the associated representations in the context of image coding. We consider only separable 2-D wavelets which are completely determined by corresponding 1-D wavelets and scaling functions.

2.1.1 Orthogonal wavelets

These are the family of wavelets that generate orthonormal bases of $\mathbf{L}^2(\mathbf{R}^n)$. Among them the most important ones to image coding are compactly supported orthogonal wavelets. In the discrete wavelet transform (DWT), compactly supported wavelets correspond to finite impulse response (FIR) filters and thus lead to efficient implementations. A systematic way of constructing compactly supported wavelets was developed by Daubechies,[15] and a fast algorithm for computing a DWT was given by Mallat.[1] Two popular families of compactly supported wavelets are the Daubechies wavelets[15] and Coifman wavelets, or Coiflets.[16] Each family is parameterized by an integer that is proportional to the length of the wavelet filter. For compactly supported wavelets, the length of a wavelet filter is related to the degree of smoothness and regularity of the wavelet, which in turn can affect the coding performance. However, studies[2,17] have found that for filter lengths greater than 8 or 10, the gain in compression performance is nominal and not worth the additional computational cost.

A major disadvantage of compactly supported orthogonal wavelets is their asymmetry. This property translates into nonlinear phase in the associated FIR filters. In computing a DWT using nonlinear phase wavelet filters and finite-length data, a periodic "wraparound" extension is often used. This may cause artifacts at the borders of the wavelet subbands. These artifacts can be avoided if we use linear-phase wavelet filters and a "flip-over" data extension.[1] Symmetry in wavelets and their associated filters can be obtained only if one is willing to give up either compact support or orthogonality of wavelets (except for the Haar wavelet). The use of noncompactly supported orthogonal wavelets such as the Lemarie–Battle wavelet in image coding has been demonstrated.[1] However, such a choice adds computational burden and is not economic in a hardware implementation of the coder. For example, although the coefficients of the Lemarie–Battle wavelet decay at an exponential rate, we found that 50 coefficients (one side) are needed to achieve a reconstruction accuracy to six significant figures. If we want both symmetry and compact support in wavelets, we are led to biorthogonal wavelets.

2.1.2 Biorthogonal wavelets

The reason for using biorthogonal wavelets is mostly for their symmetry. The price we pay for this is small as far as image coding is concerned. When using biorthogonal wavelets, the quadrature filters (QF) we use to compute a DWT are no longer an orthogonal pair. They are, however, orthogonal to another QF pair that we use to compute the inverse DWT. The perfect reconstruction property is preserved, and Mallat's fast algorithm can still be used. There are also systematic ways of constructing compactly supported biorthogonal wavelets.[18] One can choose, for example, to build filters with similar or dissimilar lengths for decomposition and reconstruction, or which are nearly orthogonal.[5] Since there is little extra cost associated with biorthogonal wavelets, they are adopted in several wavelet image coders.[5,9] A recent study by Villasenor, Bellzer, and Liao[19] compared a large number of biorthogonal wavelet filters. Although the advantages of using linear phase biorthogonal filters in image coding have been conjectured,[20] a previous study by Rioul[17] did not clearly support them.

2.1.3 Wavelet packets

Coifman, Meyer, Quake, and Wickerhauser[21] introduced wavelet packets as a generalized family of multiresolution orthogonal or biorthogonal bases that includes wavelets. A family of wavelet packet bases can be generated by the same QF pair that generate the wavelet. Extensive coverage of this topic can be found in a book by Wickerhauser.[22] From subband coding point of view, any subtree sharing the same root with the full subband tree corresponds to an orthogonal or biorthogonal representation using a specific member of the wavelet packet bases generated by a QF pair. Clearly, one can choose from this rich family a "best" basis by some criterion. Coifman and Wickerhauser[4] developed entropy-based algorithms for best basis selection. Their algorithm converges to a minimum-entropy basis. Note that the "entropy" in Coifman and Wickerhauser's algorithm is a measure of energy compaction of a vector. Another algorithm for determining the best basis in a rate-distortion sense was developed by Ramchandran and Vetterli.[10] If one is concerned primarily with lossy compression, the best basis that minimizes the total distortion for a given bit rate seems to be preferable to Coifman's minimum-entropy basis. The rationale for using a best wavelet packet basis is that it is at least as good as (if not better than) the wavelet basis for the chosen cost functional. However, there is certain cost to pay for using wavelet packets. First, extra bits are needed to encode the basis structure. Second, the resulting image coder becomes nonsymmetric in encoding and decoding; the encoder is slower because it needs to search for the best basis, which is more expensive computationally.

2.1.4 Multiwavelets

Recently, multiwavelets have been studied and used for image coding. Multiwavelets denote multiple wavelets whose dilations and translations collectively generate an orthogonal basis of $\mathbf{L}^2(\mathbf{R}^n)$. Compared with single wavelets, orthogonal multiwavelets can be shorter, with more vanishing moments, and symmetric.[23,24] An application of two wavelets to image coding was recently reported.[25] To compute a discrete multiwavelet transform (DMWT) on a scalar function, data are fed through a multirate prefilter bank followed by a multirate vector filter bank.[26] Here the prefilter bank can be viewed as a device "vectorizing" the scalar function before passing it to a multirate vector filter bank. The latter stage is an instance of vector transforms.[27,28] More specifically, it is a discrete vector-valued wavelet transform[29] similar to vector subband analysis. Vector subband coding (VSC), and more generally, vector transform coding (VTC), have been developed recently independent of wavelets.[30,31] The idea behind these developments is to match vector transforms with vector quantization techniques for best performance. Recent results suggest that this is a very promising approach to image coding.[31] It seems natural, then, to adopt vector quantization in multiwavelet transform coders, and to design matching pre- and postfilter banks as well as the vector filter banks.

2.1.5 Zero-crossings and local maxima of wavelet transforms

Under certain conditions, an image can be effectively represented by the zero crossings of the wavelet transform[32] or local maxima of the wavelet transform modulus.[12] When wavelets are carefully chosen as a smoothed gradient operator, the zero crossings and local maxima of corresponding wavelet transforms can be interpreted as "multiscale edges." Generally speaking, a nonorthogonal wavelet is required for this purpose and the resulting wavelet transform of the image is oversampled in space before the extraction of the zero crossings and local maxima. Image coding using zero crossings and local maxima was demonstrated by Mallat[32] and Mallat and Zhong.[33] The latter was refined by Froment and Mallat[34] and linked to the "second-generation image coding techniques"[35] that use image features such as contours, as coding primitives. A more recent coding system along this line was developed by Croft and Robinson.[36] These feature-based image coding systems usually require nonconventional quantization and encoding techniques. For example, in the wavelet local maxima representation, coding performance would be better if quantization were done on the chains of local maxima (edge contours) instead of individual local maxima.[12] The quantized chains of wavelet local maxima can then be encoded with a contour coder.[37]

2.2 Quantization Techniques

2.2.1 Scalar quantization (SQ)

Suppose we have decomposed an image to N dyadic scales using a wavelet transform or wavelet packet transform, either orthogonal or biorthogonal. This will yield $3N+1$ subbands in the wavelet case and a maximum of 4^N subbands in the wavelet packet case. Since the variance of each subband is generally different, we need to design a quantizer for each subband. If we assume the encoder employed at the later stage uses variable-length codewords, we are led to consider only uniform quantizers.[38] In this case the design of a uniform scalar quantizer boils down to the choice of a quantizer step size for each subband. A simple but rather arbitrary design could be to start with some step size q_0, and decrease it by a factor of 2 for all three oriented subbands as one goes to the next coarser scale. The lowest subband is often finely quantized using the smallest possible step size. The step size q_0 can be determined by matching the averaged entropy of all quantized subbands to the given total bit rate. This design is obviously nonoptimal, but works satisfactorily in practice, as evidenced by the EPIC software.[39] To increase compressibility, quantizers for higher subbands often have a dead zone that maps small coefficients (mostly due to noise) to zero.[40] More sophisticated quantizer designs can take into account the characteristics of the HVS, or an optimally allocated bit budget for each subband. Lewis and Knowles[7] designed an HVS-adapted quantizer that takes into account the HVS's spectral response, noise sensitivity in background luminance, and texture masking. If the bit budget has been allocated for each subband, then an entropy-constrained optimum quantizer can be designed.[41] The problem of optimal bit allocation in the context of wavelet image coding has been addressed in several papers.[5,42–44]

2.2.2 Vector quantization (VQ)

Vector quantization is a generalization of scalar quantization in which vectors, or blocks, of pixels are quantized instead of the pixels themselves. The general optimality of VQ over SQ was discussed by Gersho and Gray.[45] To apply VQ to wavelet image coding, the common approach is still to consider each subband individually. In the work of Antonini, Barlaud, Mathieu, and Daubechies,[5] a subcodebook is generated for each subband, and a multiresolution codebook is obtained by assembling all subcodebooks. Senoo and Girod[43] compared several VQ algorithms for subband image coding and concluded that entropy-constrained VQ gives the best performance, and that lattice VQ performs only slightly worse, but with a much simpler implementation. Since subbands are a hierarchical organization of oriented frequency bands, it is intuitive to consider quantizing a vector whose elements span subbands of the same orientation. This idea, however, does not lead to a new form of VQ; it leads to a new quantization strategy, referred to as *space quantization*.

2.2.3 Space versus frequency quantization

We refer to the technique of designing quantizers, either scalar or vector, for each individual subband as "frequency quantization" since each subband corresponds to a different frequency range. Since wavelet representations have both scale (frequency) and space contents, spatial grouping of data and quantization is possible. However, this is somewhat beyond the scope of conventional quantizer design because the number of samples corresponding to the same location in the same orientation is decreased by a factor of 4 as we move from fine to coarse scale subbands. Shapiro[11] designed an elegant method, called the *embedded zerotree wavelet algorithm (EZW)*, to turn this difficulty into an advantage. Quantization is done by successive approximation across the subbands with the same orientation. This results in an efficient data structure for encoding zero and nonzero quantized values. More recently, studies on joint space-frequency quantization[46,47] have attempted to fully exploit the space-frequency characteristics of wavelet representations.

2.3 Error-Free Encoding Techniques

2.3.1 Huffman code and run-length encoding

Although not an actual encoding technique, band based Shannon entropy is commonly used in the evaluation of coding performance. A simple encoding technique results if Huffman codes are designed for each band. Care must be exercised, however, to ensure that accurate statistics are used to design these codes. One can design a universal code based on an ensemble of typical images or explicitly transmit the Huffman codes, along with the compressed image data, to the decoder. For highly skewed sources, such as quantized wavelet transformed images, Huffman codes are known to be very inefficient. However, if the most probable symbols (zeros) are removed from the source and encoded separately, little spatial correlation remains among the nonzero values, which can then be encoded efficiently. Commonly, run-length encoding the abundance of zeros, when combined with Huffman encoding of the nonzero values, produces good results.[6,9]

2.3.2 Arithmetic Code.

Adaptive arithmetic codes start with no information about the image and implicitly transmit the model to the decoder in the compressed data stream. Therefore, they are free from the statistical ensemble issues associated with the design of Huffman codes. Binary arithmetic codes, such as the Q-code and QM-code,[48] are more computationally efficient than their multialphabet counterparts,[49] but require a mapping from the quantized coefficients to a sequence of binary decisions. A simple technique, which is similar to the run-length encoding discussed above, proves to be very beneficial. The locations of the nonzero pixels are specified by encoding a binary *activity mask* (all nonzero values are set to 1) with standard binary image compression techniques, such as the Joint Bi-level Image Experts Group (JBIG) coder, after which the nonzero pixels are mapped through a balanced binary tree and encoded. Using this *color shrinking*[50] based technique, we often obtain bit rates less than the Shannon entropy (based on independent pixels) due to the significant spatial correlation between the zeros in a wavelet-transformed image. An alternative, efficient representation of the zeros in the source is exploited by Shapiro's zerotree[11] coder.

3 PICTURE QUALITY SCALE

Research into the psychophysics of human visual perception has revealed that the HVS is not equally sensitive to various types of distortion in an image. This directly affects the perceived image quality. The PQS is based on quantitative measures of several distortion factors. Because these distortion factors are correlated, a principal component analysis is done to transform them into uncorrelated "sources of errors," and dominant sources are identified. These errors are then mapped to a PQS value by a model which was obtained from a linear regression analysis with the mean opinion score.

3.1 Distortion Factors

The current version of the PQS includes five distortion factors of which the first two are derived from random errors and the last three from structural errors. Here we give only a description of these distortion factors. Formulas for computing the actual numerical measures are detailed in two references.[14,51,52] Perceptual distortion measures depend on the viewing distance that here is assumed to be four times the picture height.

Distortion factor F_1 is a weighted difference between the original and the compressed images. The weighting function adopted is the International Radio Consultative Committee (CCIR) television noise weighting standard.

Distortion factor F_2 is also a weighted difference between the original and the compressed images. The weighting function is from a model of the HVS. In addition, an indicator function is included to account for the perceptual threshold of visibility.

Table 1: Covariance matrix of F_i

	F_1	F_2	F_3	F_4	F_5
F_1	1.00	0.97	0.95	0.03	0.97
F_2	0.97	1.00	0.99	0.15	0.91
F_3	0.95	0.99	1.00	0.17	0.88
F_4	0.03	0.15	0.17	1.00	0.11
F_5	0.97	0.91	0.88	0.11	1.00

Table 2: Scales of the MOS

Grading Scales	Impairment
5	Imperceptible
4	Perceptible, but not annoying
3	Slightly annoying
2	Annoying
1	Very annoying

Distortion factor F_3 reflects the end-of-block disturbances. The HVS is quite sensitive to linear and structured error features in images. In block coders, the error image contains discontinuities at the end of blocks, which explains perceived blocking artifacts in the compressed image.

Distortion factor F_4 accounts for general correlated errors. Errors with strong correlation are more perceptible than random patterns. The error image having strong correlation suggests more apparent distortion in the image to human viewers than accounted for by the magnitude of the errors.

Distortion factor F_5 is a measure of the large errors that occur for most coders in the vicinity of high contrast transitions (edges). Two psychophysical effects occur in the vicinity of high contrast edges. On the one hand, the visibility of noise and errors decreases; this is referred to as *visual masking*. On the other hand, the visibility of misalignments increases.

3.2 Principal Component Representation of Distortion Measures

Because the distortion factors $\{F_i\}_{1\leq i\leq 5}$ are correlated, a principal component analysis is performed to decorrelate the distortion measures and identify the dominant sources. This is done for a test set of distorted images obtained from representative coders. Table 1 lists a covariance matrix of $\{F_i\}$, C_F. It was computed from a set of 24 distorted images obtained by encoding two reference images with transform and DPCM coders for a range of quality. The two reference images are "Hairband" and "Church" specified by the Institute of Television Engineers (ITE) of Japan. Our experiments with a large number of other images indicated that this estimate of C_F is quite robust: its elements have no significant changes for different test images. An eigen analysis on C_F gave the transform matrix that decorrelates $\{F_i\}$. It was found out that among the five eigenvalues of C_F the three largest ones account for 98% of the total error energy. Therefore, the three eigenvectors corresponding to the three largest eigenvalues can be chosen to transform $\{F_i\}$ into a principal component representation, $\{Z_i\}_{1\leq i\leq 3}$.

3.3 Formation of the PQS

Since the various distortion factors collectively contribute to the overall perceived image quality, we seek a functional model mapping the distortion factors or measures to a single quality scale, the PQS. This model can be experimentally determined by studying the functional relationship between the distortion measures and the MOS, a five scale subjective ranking of image quality in terms of perceived distortions that are described in Table 2.[53] The simplest model is a linear one in which the PQS is expressed as a linear combination of uncorrelated principal distortion measures, $\{Z_i\}$, that is,

$$PQS = b_0 + \sum_{i=1}^{3} b_i Z_i$$

where $\{b_i\}_{0\leq i\leq 3}$ are the partial regression coefficients obtained by multiple linear regression of $\{Z_i\}$ against the MOS.[51,52,54] Nonlinear models have also been studied that employ neural networks to compute the PQS.[55,56]

For the aforementioned set of 24 distorted images, the MOS values were obtained from an experiment involving nine observers under the conditions specified by the CCIR.[53] The observers were allowed to give half scale scores. A multiple linear regression analysis of $\{Z_i\}$ against the MOS gave $b_0 = 6.431$, $b_1 = -0.069$, $b_2 = -1.475$, $b_3 = -0.136$, with the correlation coefficient $R = 0.88$. Our extensive experiments indicate that PQS differentiates images encoded at the same signal-to noise ratio (SNR), in accordance with the assessment of image quality by human observers.

4 RESULTS AND REMARKS

4.1 About the Experiment

In this section we present some results from our comparative study of several wavelet coders. The comparison is in the rate-distortion sense where the distortion is measured by both PQS and PSNR. Two popular test images, "Lena" and "Barbara," both 512×512, were used in the experiment. A total of 760 encoded images were compared, representing a combination of two wavelets, three quantizers, and three encoders, plus the EZW coder, for coding the two test images at 20 bit rates ranging uniformly from 0.1 to 2.0 bits/pixel. The two wavelets used are the orthogonal, 8-tap wavelet of Daubechies (D8)[15] and the biorthogonal, "9-7" wavelet of Barlaud (B97).[5,20] The motivation for choosing these two specific wavelets for our comparative study is explained in the next section. All wavelet transforms are computed for four dyadic scales, resulting in 13 subbands. All three quantizers are scalar quantizers: the first is the nonoptimized quantizer (Q1) described in Sec. 2.2; the second is the HVS-adapted quantizer (Q2) of Lewis and Knowles[7]; the third is an entropy-constrained quantizer (Q3) in which a bit budget is optimally allocated to each subband and used as a constraint in the quantizer design; we have used the optimum bit allocation scheme of Chen, Itoh, and Hashimoto[42] with a uniform Laplacian rate-distortion model.[38] All three encoders are band based, i.e., each band is processed separately. They are a simple Huffman encoder (E1), run-length encoded zeros plus Huffman encoded nonzero values (E2), and the activity mask based technique discussed in Sec. 2.3, where we QM-encode the mask using a 7-pixel spatial predictive context and the nonzero values using binary tree decomposition (E3). In addition, we tested the EZW coder with the B97 wavelet, tree-structured spatial quantization, and adaptive arithmetic encoding.

The results are computed, organized, and presented in several ways. In assessing the choice of wavelets and quantizers, we use the computed entropy H of a quantized wavelet representation as the bit rate, assuming we have an ideal entropy encoder. In the coding experiment, we adjusted the quantizers so that the entropy of a quantized wavelet-transformed image matches (within 0.005 error bound) the target nominal bit rate. The two wavelets {B97,D8} are compared for fixed quantizers and the three quantizers {Q1,Q2,Q3} are compared for fixed wavelets. To compare the three encoders {E1,E2,E3}, we encode images quantized at the nominal bit rates H, compute the actual output bit rates, and then plot them against H (which is the lower bound on bit rate if the pixels are independent). Finally, we compare the overall performance of a few coders synthesized from different choices of wavelets, quantizers, and encoders. We do this by plotting PQS and PSNR versus actual bit rates for each assembled coder. Owing to the large amount of data, we use both tables and graphs to present our results.

4.2 Comparison of Two Wavelets

In theory, we have a large number of candidates from the families of orthogonal and biorthogonal wavelets that can be used for image coding. In practice, designers often focus on a small number of candidates. We have chosen two commonly used wavelet filters for our comparative study, B97 and D8, one from each family. These filters are comparable in length (8 taps on average) and represent a good tradeoff among smoothness, regularity, and computational cost. A recent study by Villasenor, Bellzer, and Liao[19] rated B97 first for overall performance among a large number of biorthogonal wavelet filters. Therefore, although we cannot make conclusive comparisons between orthogonal and biorthogonal wavelets, we feel that our comparison of B97 and D8 is representative.

Fig. 1 contains four plots comparing B97 with D8 for quantizer Q2, Similar results are found for quantizers

Q1 and Q3; we tabulate these results in Tables 3 and 4. In all cases B97 leads D8 in both PQS and PSNR for a large portion of our test bit rate range. For a given bit rate, the lead of B97 over D8 can be as much as 0.39 PQS or 1.2 dB. From another point of view, using B97 one can save as much as approximately 0.2 bits/pixel for a given PQS or PSNR value. Note that the filters of B97 and D8 have similar lengths; the advantage of the former over the latter is clear in this experiment.

4.3 Comparison of Three Quantizers

Fig. 2 compares our three quantizers for wavelet B97. Again, numerical results can be found in Tables 3 and 4 for both B97 and D8. We see little difference between the three quantizers if we look at the PSNR plots in Fig. 2 or compare the corresponding figures in Tables 3 and 4. The PQS comparisons, however, tell a different story. We find that Q2 is best in most cases. For low bit rates, Q2 is sometimes slightly outmatched by one of the other quantizers. At higher rates, the dominance of Q2 increases to as much as 0.36 PQS for "Barbara." The relationship between Q1 and Q3 in PQS seems image dependent. With its PQS values close to those of Q2, Q3 clearly outperforms Q1 for "Lena," but the competition appears tied for "Barbara." In Figs. 3 and 4, we give a visual comparison of compressed-decompressed images by the three quantizers at the nominal bit rate (entropy) of 0.5 bits/pixel. Examination of these images reveals that Q2 results in better visual quality, which agrees with the PQS ratings. Recall that Q2 is an HVS-adapted quantizer. Its advantage is not obvious at all from PSNR values. The PQS confirms the value of the HVS-adapted quantization.

We observe that the nonoptimized quantizer Q1 performs quite well. This is not surprising because the step sizes of Q1 are not completely arbitrary. The variances of wavelet coefficients in subbands are generally unequal. A rule of thumb based on equal quantization MSE in each subband suggests that the bits allocated to the subband should be proportional to the logarithm of its variance. This implies that the number of quantization levels should be proportional to the variance, and in the case of uniform quantization, the quantizer step size should be inversely proportional to the variance. For many images, the variances of subbands increased in going from fine to coarse scales. The step sizes of Q1 are based upon such an observation; they would be near optimal if the variances in oriented subbands increased by a factor of 2 from fine to coarse scales. From another point of view, Q1 can be shown to be optimal if the wavelet coefficients in each subband are uniformly distributed.[42]

4.4 Comparison of Three Encoders

Fig. 5 shows the output bit rates of three encoders versus computed entropies for "Lena" and "Barbara." Similar results were observed for all wavelets and quantizers; therefore we averaged the results across wavelets and quantizers to produce the composite results shown in Fig. 5. For reference, all results including nonaveraged output bit rates from three encoders for "Lena" and "Barbara" are tabulated in Tables 5 to 10.

In each plot of Fig. 5 we also draw a line of unit slope where the output bit rate equals the entropy. As expected, the simple Huffman encoder (E1) always gives a bit rate higher than the entropy, especially at low bit rates where there are a large number of zeros, i.e., when the source is highly skewed. When combined with run-length encoding of the zeros (E2), the results are much better, and only slightly worse than our best, the activity mask based technique. We must point out, though, that our Huffman code results are image specific and do not include the overhead of transmitting 13 (one per subband) Huffman codes to the decoder. Therefore, the bit rates for E1 and E2 in Fig. 5 are lower bounds on the rate of a more realistic code. We did not compute the cost of transmitting the Huffman codes or consider the design of a generic Huffman code based on an appropriate ensemble of images because the results for code E3 are better and do not ignore any hidden costs. We observe that the bit rates for E3 are consistently lower than the (independent pixel) entropy, which may appear counterintuitive to some, but is correct since we are exploiting spatial dependencies in the source which are not reflected in the entropy computation. Note that by using E3 we can obtain bit rates as much as 0.25 bits/pixel below the entropy for "Barbara," or 0.1 bits/pixel for "Lena." We declare E3 the winner.

4.5 Comparison of Wavelet Coders

We now compare a few complete wavelet image coders synthesized from different wavelets, quantizers, and encoders. A combination of "the best" gives the B97-Q2-E3 for both "Lena" and "Barbara." We also present D8-Q1-E1 and D8-Q2-E3 for both test images. These coders along with the EZW coder are compared in Fig. 6. We see that for both "Lena" and "Barbara," B97-Q2-E3 is the winner by PQS for most bit rates, with EZW winning at high bit rates. By PSNR, B97-Q2-E3 still wins for "Barbara," but loses to EZW by a small margin for "Lena." Note that the scalloped behavior of the EZW performance curve is due to the use of a fixed value ($M = 1.0$) for the minimum slice threshold in Shapiro's algorithm.[11] To obtain the best results, a costly optimization of this parameter would be required at each bit rate. Also observed from Fig. 6, the simple Huffman encoder yields, clearly, the poorest coder for both test images and by both PQS and PSNR. The performance difference between the best (B97-Q2-E3) and the worst (D8-Q1-E1) coders can be as large as 2.6 in PQS or 9 dB in PSNR for "Barbara." Of course, an intelligent designer would not choose such a code. Our results only indicate how bad such a brute force design can be. The only difference between coders D8-Q2-E3 and B97-Q2-E3 is the choice of wavelets. As such, the orthogonal wavelet based coder, D8-Q2-E3, performs slightly worse than the biorthogonal wavelet based coder, B97-Q2-E3. In Fig. 7, we give a visual comparison of "Lena" coded at approximate 0.17 bits/pixel by B97-Q2-E3, D8-Q2-E3, and the EZW coders. Note that at this rate, the image quality is so low that the PQS values fall out of the valid range. The PSNR figures, however, are indicative in this case.

Coders representing other combinations can also be synthesized. Their performance can be evaluated by combining columns in Table 3 or 4 with columns in Tables 5,7,9 or 6,8,10, for "Lena" and "Barbara," respectively. For example, to examine the performance of coder B97-Q2-E2 for "Lena," we look up and plot columns 4 and 5 in Table 3 against column 3 in Table 7. Since we have plotted the best and worst overall cases in Fig. 6, we expect all other combinations to produce results between that of B97-Q2-E3 and D8-Q1-E1.

4.6 Remarks

Earlier, we reported some comparative results using only PQS for "Lena" and "Barbara" of lower resolution (256×256).[57] The results presented here appear to be generally consistent with our previous results, though there are slight differences.

The purpose of our comparative study is not to simply rank a number of coders. We hope to find out why a coder is good or bad and how to make a good coder. The EZW coder is, in our mind, the state-of-the-art technique in wavelet image coding. The fact that we can make a coder that comes close to or is even better than the EZW coder just by assembling available techniques testifies to the value of good synthesis in wavelet coder design. Our results clearly show that all parts (representation, quantization, and error-free encoding) are important in designing wavelet coders. Since wavelets were introduced to image coding, there has been considerable research looking for better wavelets. The close and good performance of D8-Q2-E3 and B97-Q2-E3 in our study suggests that the effect of different wavelets (of similar filter lengths) may be less significant than that of quantizers and encoders. We have evaluated three representative scalar quantizers. Among them the HVS-adapted quantizer is particularly attractive, because after all, most compressed images are intended for human viewers upon decompression. We have not included the large family of vector quantizers here. We felt that they warrant another comparative study. Naturally, multiwavelets can be included in such a study.

The efficiency of error-free encoders is another important issue. The shift of curves (except EZW) from the nominal bit rate range in Fig. 6 indicates the performance gain or loss due to encoder efficiency. We have shown that a good encoder (e.g., E3) can achieve a bit rate lower than the (independent pixel) entropy, making the curve shift to the right in Fig. 6. On the other hand, an inefficient encoder (E1) produces a bit rate much higher than the entropy, making the curve shift to the left. The key to a good encoder is to exploit dependency between pixels. This in turn calls for a good data structure organizing wavelet transformed data. Comparing EZW with B97-Q2-E3, we found that both exploit dependencies between the quantized coefficients, which allows them to achieve bit rates below the entropy. The difference is that the EZW exploits both intra- and interband dependencies by encoding the zerotrees while B97-Q2-E3 exploits more intraband dependency by encoding the activity masks. In

additional, the EZW coder is a good example of intelligent organization of data for quantization and encoding.

The PQS quantifies some perceptual characteristics of a coder that can not be revealed by the PSNR; see, e.g., quantizer comparisons in Sec. 4.3. This makes the PQS an attractive alternative to PSNR as a distortion measure. However, the PQS is a relatively coarse scale that has only five defined levels. So although the computation can give PQS values between these levels (e.g. 4.1, and 4.2), their perceptual meanings are not well defined. This reflects the fact that the PQS is constructed by regression with MOS, which is a 5-level grading scale. A 0.1 resolution on MOS scale would mean that 40 grading levels are meaningful. Perhaps few human observers can do such a fine grading. Thus to improve the "perceptual resolution" of the PQS, we need to map it to other perceptual metrics. We also note that the PQS versus entropy (or bit rate) curves are relatively flat at high bit rates but become increasingly steep at low bit rates and can fall out of the valid range to become meaningless. This reflects the nonlinearity in perception. That is, human observers have certain tolerance for moderately distorted images. Once the distortion becomes annoying, the perceived image quality falls rapidly. The lesson to the designers then is to make a coder that maximizes the bit rate range in which the PQS curve is above the knee.

5 CONCLUSION

We have presented some results from a comparative study of different wavelet image coders using a perception-based picture quality scale as well as the traditional PSNR. While our study cannot cover all the aspects of wavelet coder design, we believe that the comparisons we made are highly representative. These results can provide a reference by which application developers can choose a good wavelet coder for their applications, as well as shed some light on the design of wavelet coders. Our work shows that an excellent wavelet coder can result from a careful synthesis of existing techniques of wavelet representation, quantization, and error-free encoding. All three parts play a role in making a good coder. Exploiting the dependency of quantized coefficients, including zeros, is an effective way to boost the overall performance of a wavelet coder. Quantizers designed with considerations of the characteristics of HVS are very attractive; their advantages can be quantified when an appropriate distortion measure is used. The effect of variations between asymmetric orthogonal and symmetric biorthogonal wavelets is also noticeable, but seems less significant when compared with the other two factors. Finally, our study testifies to the necessity of perception-based quality metrics such as the PQS for coder evaluation. The approach we take here is certainly not limited to evaluation of wavelet coders.

6 ACKNOWLEDGMENT

We would like to thank A. Kris Huber of Utah State University for providing us with his implementation of the EZW coder. We also acknowledge support of the UC Micro Program, Hewlett-Packard, Lockheed, and Pacific Bell.

7 REFERENCES

[1] S. G. Mallat, "A theory of multiresolution signal decomposition: the wavelet representation," *IEEE Trans. Pattern Anal. and Machine Intell.*, vol. PAMI-11, pp. 674-693, July 1989.

[2] W. R. Zettler, J. Huffman, and D. C. P. Linden, "Application of compactly supported wavelets to image compression," *Proceedings of SPIE, Image Processing Algorithms and Applications,* vol. 1244, pp. 150-160, 1990.

[3] R. A. DeVore, B. Jawerth, and B. J. Lucier, "Image compression through wavelet transform coding," *IEEE Trans. on Information Theory*, vol. 38, pp. 719-746, Mar. 1992.

[4] R. R. Coifman and M. V. Wickerhauser, "Entropy-based algorithms for best basis selection," *IEEE Trans. Infor. Theory*, vol. 38, pp. 713-718, Mar. 1992.

[5] M. Antonini, M. Barlaud, P. Mathieu, and I Daubechies, "Image coding using wavelet transform," *IEEE Trans. on Image Processing*, vol. 1, pp. 205-220, Apr. 1992.

[6] J. N. Bradley, C. M Brislawn, and T. Hopper, "The FBI wavelet/scalar quantization standard for grayscale fingerprint image compression," *Proc. of SPIE, Visual Info. Proc. II*, vol. 1961, pp. 293-304, 1992.

[7] A. S. Lewis and G. Knowles, "Image compression using the 2-D wavelet transform," *IEEE Trans. on Image Processing*, vol. 1, pp. 244-250, Apr. 1992.

[8] M. Ohta, M, Yano, and T. Nishitani, "Wavelet picture coding with transform coding approach," *IEICE Trans. Fundamentals*, vol. E75-A, pp. 776-785, July 1992.

[9] C. K. Cheong, K. Aizawa, T. Saito, and M. Hatori, "Subband image coding with biorthogonal wavelets," *IEICE Trans. Fundamentals*, vol. E75-A, pp. 871-881, July 1992.

[10] K. Ramchandran and M. Vetterli, "Best wavelet packet bases in a rate-distortion sense," *IEEE Trans. Image Processing*, vol. 2, pp. 160-175, Apr. 1993.

[11] J. M. Shapiro, "Embedded image coding using zerotrees of wavelet coefficients," *IEEE Trans. on Signal Proc.*, vol. 41, pp. 3445-3462, Dec. 1993.

[12] S. G. Mallat and S. Zhong, "Characterization of signals from multiscale edges," *IEEE Trans. Pattern Anal. and Machine Intell.*, vol. PAMI-14, pp. 710-732, July 1992.

[13] S. G. Mallat, "Multifrequency channel decomposition of images and wavelet models," *IEEE Trans. Acoust. Speech and Signal Proc.*, vol. 37, pp. 2091-2110, Dec. 1989.

[14] V. R. Algazi, Y. Kato, M. Miyahara, and K. Kotani, "Comparison of image coding techniques with a Picture Quality Scale," *Proceedings of SPIE, Applications of Digital Image Processing XV*, vol. 1771, pp. 396–405, 1992.

[15] I. Daubechies, "Orthonormal bases of compactly supported wavelets," *Comm. Pure Appl. Math.*, vol. 41, pp. 909-996, 1988.

[16] I. Daubechies, "Orthonormal bases of compactly supported wavelets II, Variations on a theme," *SIAM J. Math. Anal.*, vol. 24, pp. 499-519, Mar. 1993.

[17] O. Rioul, "On the choice of 'wavelet' filters for still image compression," *Proceedings of ICASSP'93*, vol. V, pp. 550-553, 1993.

[18] A. Cohen, I. Daubechies, and J.-C. Feauveau, "Biorthogonal bases of compactly supported wavelets," *Comm. Pure Appl. Math.*, vol. 45, pp. 485-500, 1992.

[19] J. D. Villasenor, B. Bellzer, and J. Liao, "Wavelet filter evaluation for image compression," *IEEE Trans. on Image Processing*, vol. 4, No. 8, pp. 1053-1060, Aug. 1995.

[20] I. Daubechies, *Ten Lectures on Wavelets*, SIAM, Philadelphia, PA, 1992.

[21] R. R. Coifman, Y. Meyer, S. R. Quake, and M. V. Wickerhauser, "Signal processing and compression with wavelet packets," in *Proc. of Intl. Conf. on Wavelet Applications*, Toulouse, France, 8-13 June 1992, pp.77-93.

[22] M. V. Wickerhauser, *Adapted Wavelet Analysis from Theory to Software*, A K Peters, Wellesley, MA, 1994.

[23] P. R. Massopust, J. S. Geronimo, and D. P. Hardin, "Fractal functions and wavelet expansions based on several scaling functions," *Journal of approximation theory*, v. 78, no. 3, pp. 373-401, Sept. 1994.

[24] G. Strang and V. Strela, "Orthogonal multiwavelets with vanishing moments," *Optical Engineering*, v. 33, No. 7, pp. 2104-2107, July 1994.

[25] P. N. Heller, V. Strela, G. Strang, P. Topiwala, C. Heil and L. S. Hills, "Multiwavelet filter banks for data compression," in IEEE Symp. on Circuits and Systems, pp. 1796–9, 1995.

[26] X.-G. Xia, J. S. Geronimo, D. P. Harding, and B. W. Suter, "Design of prefilters for discrete multiwavelet transform," in *IEEE Trans. Signal Proc.*, 44, 25–35, 1996.

[27] W. Li, "Vector transform and image coding," *IEEE Trans. Circuits and Syst. for Video Tech.,* vol. 1, pp. 297-307, Dec. 1991.

[28] W. Li, "On vector transformation," *IEEE Trans. Signal Proc.,* vol. 41, pp. 3114-3126, Nov. 1993.

[29] X.-G. Xia and B. W. Suter, "Vector-valued wavelets and vector filter banks," in *IEEE Trans. Signal Proc.*, 44, 508–18, 1996.

[30] W. Li and Y.-Q. Zhang, "A study of vector transform coding of subband decomposed images," *IEEE Trans. Circuits and Syst. for Video Tech.*, vol. 4, Aug. 1994.

[31] W. Li and Y.-Q. Zhang, "Vector-based signal processing and quantization for image and video compression," *Proc. of IEEE*, vol. 83, no. 2, pp. 317-335, Feb. 1995.

[32] S. G. Mallat, "Zero-crossings of a wavelet transform," *IEEE Trans. Inform. Theory*, vol. IT-37, pp. 1019-1033, July 1991.

[33] S. G. Mallat and S. Zhong, "Compact image coding from multiscale edges," in *Proc. Intl. Conf. Acoust. Speech and Signal Proc.*, Toronto, May 1991.

[34] J. Froment and S. Mallat, "Second generation compact image coding with wavelets," in *Wavelet: A Tutorial in Theory and Applications,* C.K. Chui, Ed., Academic Press, San Diego, 1992.

[35] M. Kunt, A. Ikonomopoulos and M. Kocher, "Second-generation image-coding techniques," *Proc. of IEEE*, vol. 73, pp. 549-574, April, 1985.

[36] L. H. Croft and J. A. Robinson, "Subband image coding using watershed and watercourse lines of the wavelet transform," *IEEE Trans. Image Proc.*, vol. 3, pp. 759-772, Nov. 1994.

[37] S. Carlsson, "Sketch based coding of grey level images," *Signal Processing*, vol. 15, pp. 57-83, 1988.

[38] A. K. Jain, *Fundamentals of Digital Image Processing*, Prentice-Hall, Englewood Cliffs, NJ, 1989.

[39] E. P. Simoncelli and E. H. Adelson, "Efficient Pyramid Image Coder (EPIC)," a public domain software available from URL: ftp://whitechapel.media.mit.edu/pub/epic/epic.tar.Z

[40] M. Vetterli and J. Kovačević, *Wavelets and Subband Coding*, Englewood Cliffs, NJ, Prentice Hall PTR, 1995.

[41] R. C. Wood, "On optimum quantization," *IEEE Trans. Infor. Theory,* vol. IT-15, pp. 248-252, Mar. 1969.

[42] J. Chen, S. Itoh, and T. Hashimoto, "Scalar quantization noise analysis and optimal bit allocation for wavelet pyramid image coding," *IEICE Trans, Fundamentals,* vol. E76-A, pp. 1502-1514, Sep. 1993.

[43] T. Senoo and B. Girod, "Vector quantization for entropy coding of image subbands," *IEEE Trans. Image Proc.*, vol. 1, pp. 526-533, Oct. 1992.

[44] R. R. Matic and J. I. Mosley, "Wavelet transform-adaptive scalar quantization of multispectral data," in *Proc. of AIAA Computing in Aerospace 9 Conference,* San Diego, Oct. 1993.

[45] A. Gersho and R. M. Gray, *Vector Quantization and Signal Compression*, Kluwer Academic Publishers, Boston, 1992.

[46] Z. Xiong, K. Ramchandran, and M. T. Orchard, "Joint optimization of scalar and tree-structured quantization of wavelet image decompositions," *Proc. 27th Annual Asilomar Conf. on Signal, Syst. and Computers*, Pacific Grove, CA, Nov. 1993, pp. 891-895.

[47] Z. Xiong, K. Ramchandran, M. T. Orchard, and K. Asai, "Wavelet packets-based image coding using joint space-frequency quantization," *Proc. IEEE Intl. Conf. Image Proc.*, Austin, TX, Nov. 1994, vol. III, pp. 324-328.

[48] W. B. Pennebaker, J. L. Mitchell, G. G. Landon, Jr., and R. B. Arps, "An overview of the basic principles of the Q-coder adaptive binary arithmetic coder," *IBM J. Research and Development*, vol. 32 pp. 717-726, Nov. 1988.

[49] I. H. Witten, R. M. Neal, and J. G. Cleary, "Arithmetic coding for data compression," *Comm. ACM*, vol. 30, pp. 520-539, June. 1987.

[50] V. R. Algazi, P. L. Kelly, R. R. Estes, "Compression of binary facsimile images by preprocessing and color shrinking." *IEEE Transactions on Communications*, vol. 38, No. 9, pp. 1592–1598, 1990.

[51] M. Miyahara, K. Kotani, and V. R. Algazi, "Objective Picture Quality Scale (PQS) for Image Coding," *Proc. SID Symposium for Image Display*, 44.3: pp. 859-862, May 1992.

[52] M. Miyahara, K. Kotani, and V. R. Algazi, "Objective Picture Quality Scale (PQS) for Image Coding," submitted to IEEE Trans. on Communications, May 1996.

[53] CCIR, "Rec. 500-2, Method for the subjective assessment of the quality of the television pictures," vol. 11, pp. 165-168, 1982.

[54] M. Miyahara, K. Kotani, Y. Horita, and T. Fujimoto, "Objective Picture Quality Scale (PQS)—Consideration of local feature and universality," *IEICE Trans. B-I,* vol. J73-B-I, pp. 208-218, Mar. 1990. (in Japanese).

[55] K. Kotani and M. Miyahara, "Objective picture quality scale by neural network (PQS-NN)," *IEICE Trans. B-I*, vol. J73-B-I, pp. 347-352, Apr. 1990. (in Japanese).

[56] K. Kotani and M. Miyahara, "Objective picture quality scale by neural network fed the distortion factors to the input layers," *IEICE Trans. D-II*, vol. J73-D-II, pp. 1303-1308, Aug. 1990. (in Japanese).

[57] J. Lu, V. R. Algazi, and R. R. Estes, "Comparison of wavelet image coders using the Picture Quality Scale (PQS)," in *Wavelet Applications II*, H.H. Szu, Editor, *Proc. of SPIE*, vol. 2491, pp. 1119-1130, Apr. 1995.

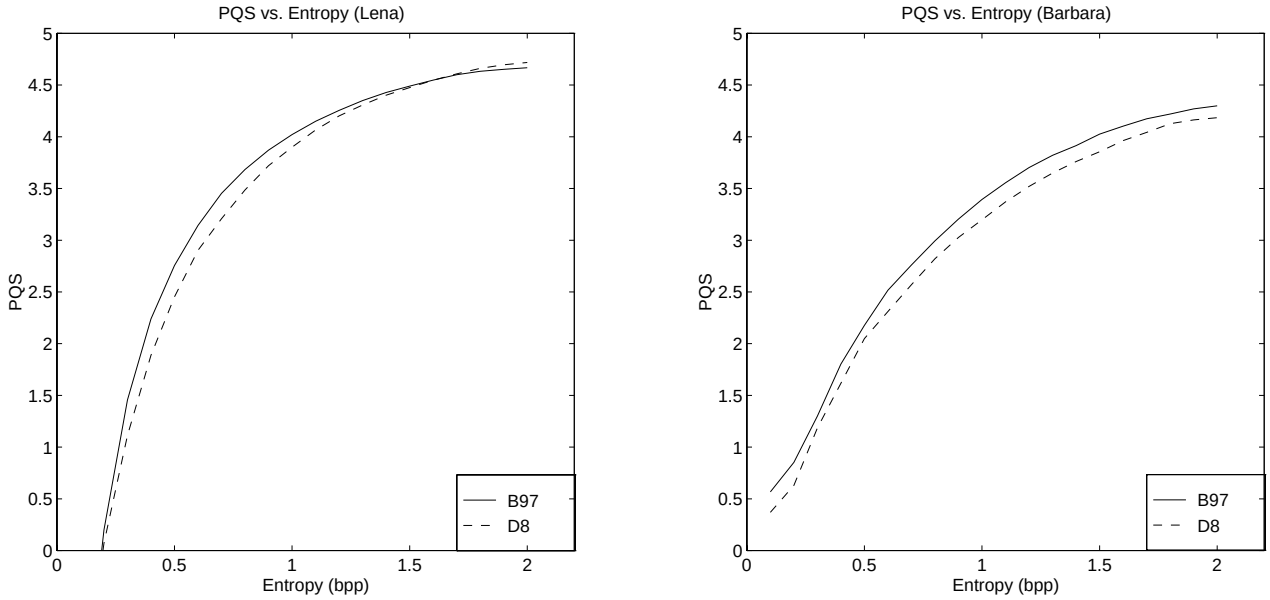

(a)

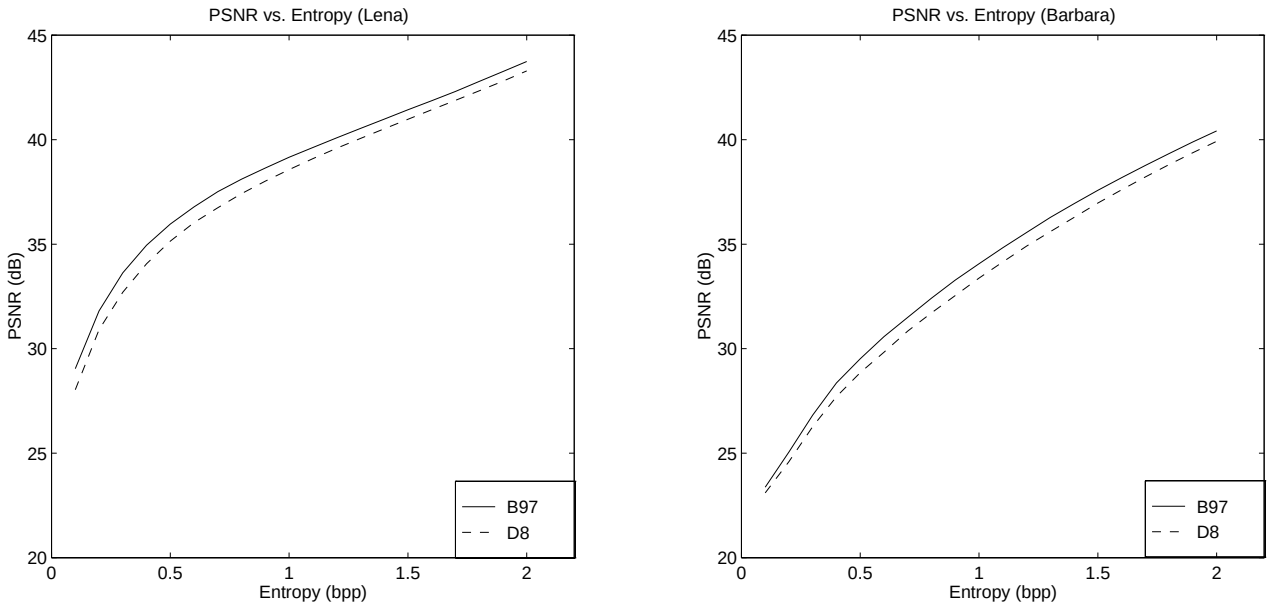

(b)

Figure 1: Comparison of two wavelets, {B97,D8}, under quantizer Q2. Left and right charts are for "Lena" and "Barbara," respectively: (a) comparison by PQS and (b) comparison by PSNR.

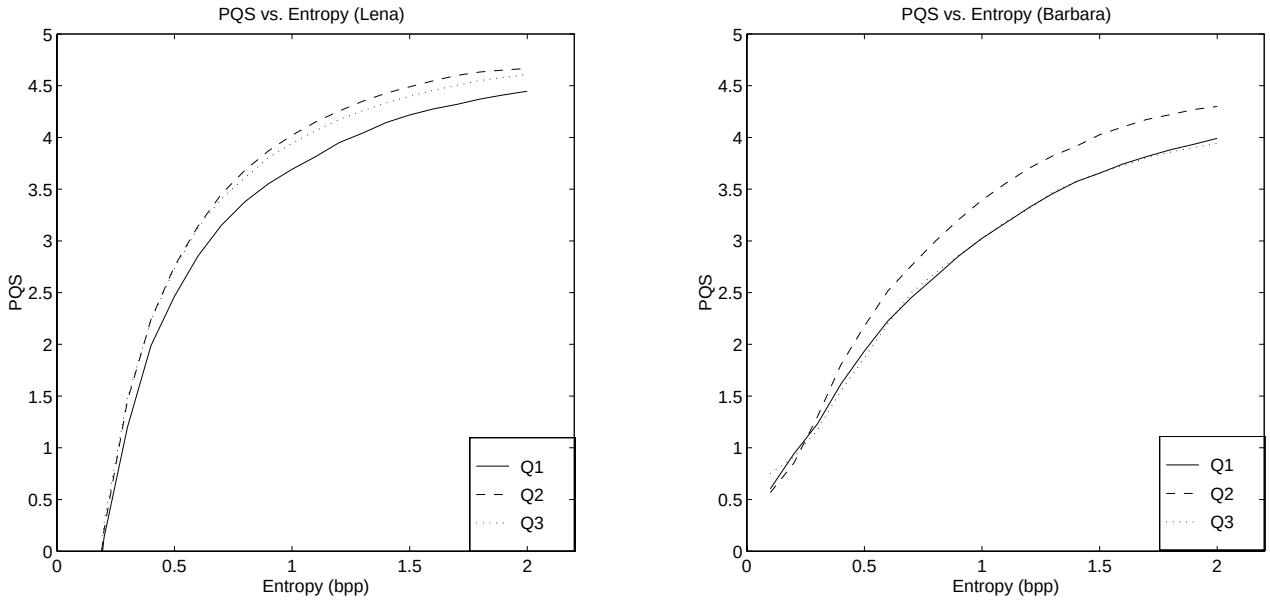

(a)

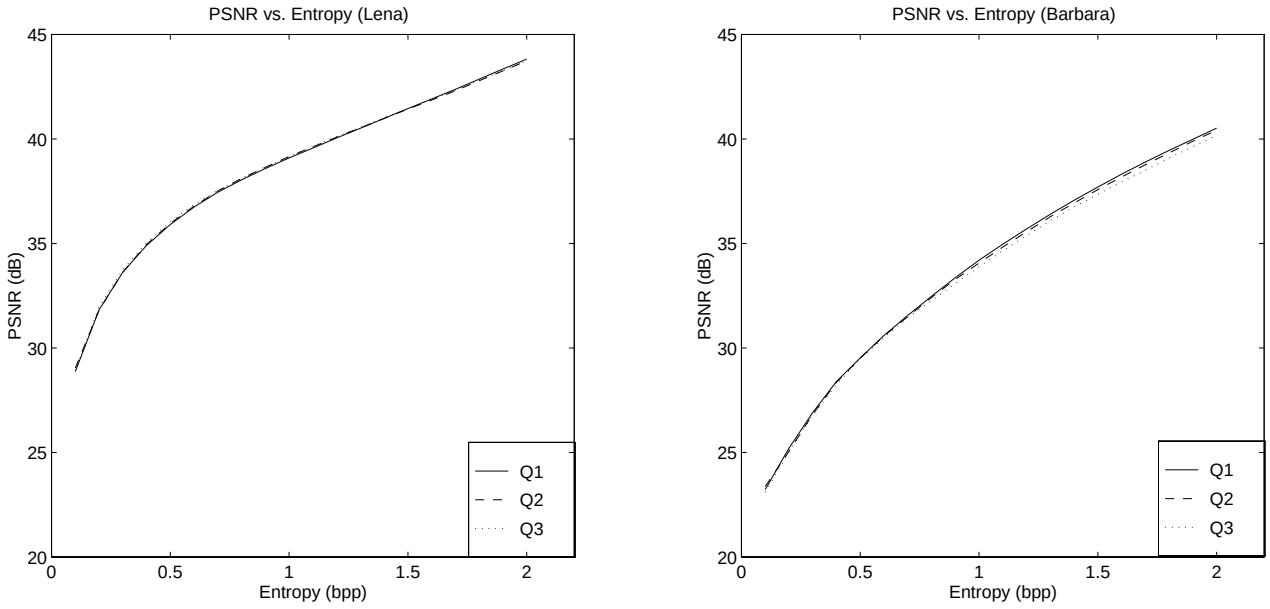

(b)

Figure 2: Comparison of three quantizers, {Q1,Q2,Q3}, under wavelet B97. Left and right charts are for "Lena" and "Barbara," respectively: (a) comparison by PQS and (b) comparison by PSNR.

original

Q1 (1.9 PQS/29.5 dB)

Q2 (2.2 PQS/29.5 dB)

Q3 (1.9 PQS/29.5 dB)

Figure 3: A visual comparison of "Barbara" compressed-decompressed with three quantizers, {Q1,Q2,Q3}, and wavelet B97. A portion (boxed) of the image is enlarged and compared in Figure 4.

original

Q1 (1.9 PQS/29.5 dB)

Q2 (2.2 PQS/29.5 dB)

Q3 (1.9 PQS/29.5 dB)

Figure 4: A visual comparison of an enlarged portion of "Barbara" compressed-decompressed with the three quantizers, {Q1,Q2,Q3}, and wavelet B97. From left to right and top to bottom are the original, Q1, Q2, and Q3. The full-sized images are shown in Figure 3.

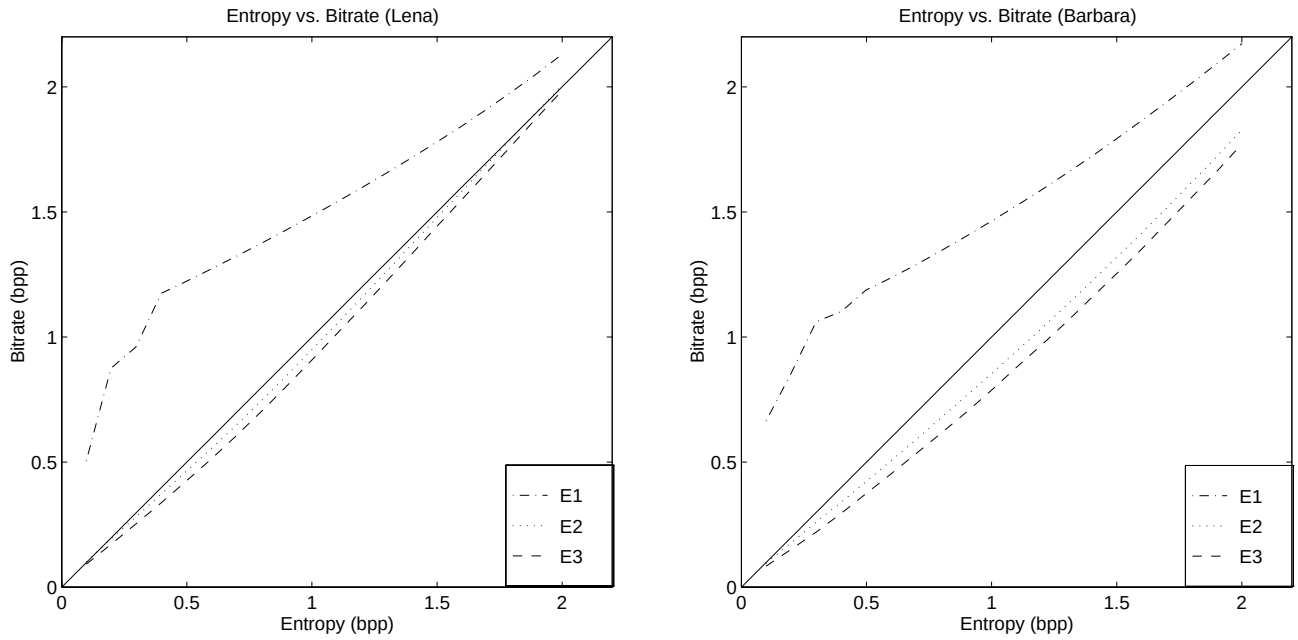

(a) (b)

Figure 5: Comparison of three encoders, {E1,E2,E3}. Bit rates are averaged over {B97,D8} and {Q1,Q2,Q3} for the same images: (a) comparison for "Lena" and (b) comparison for "Barbara."

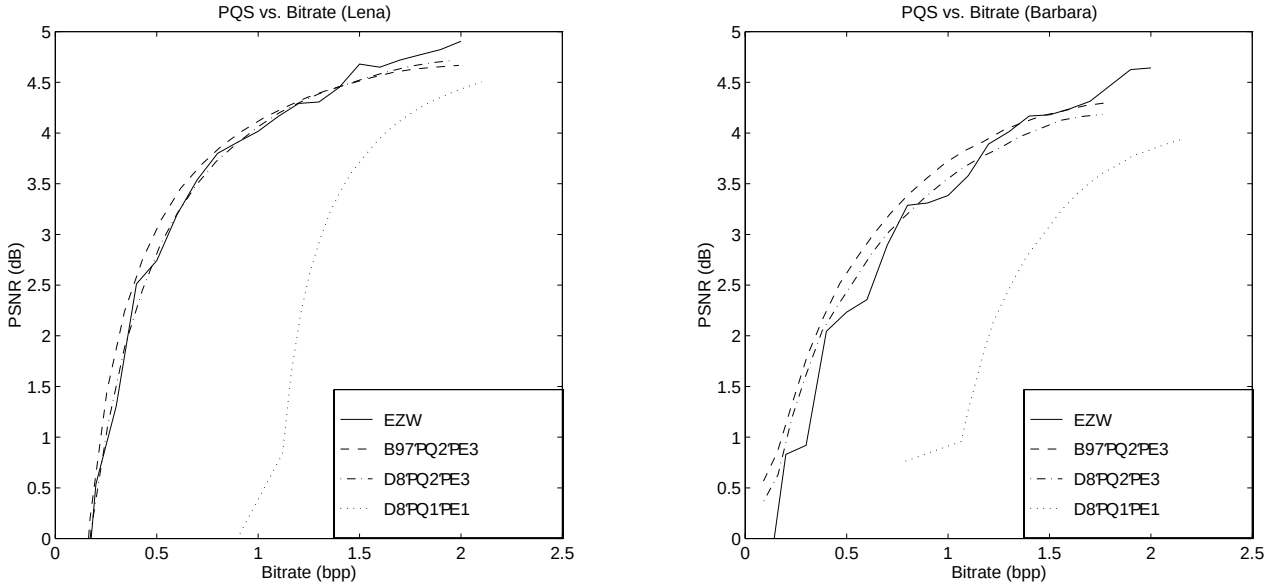

(a)

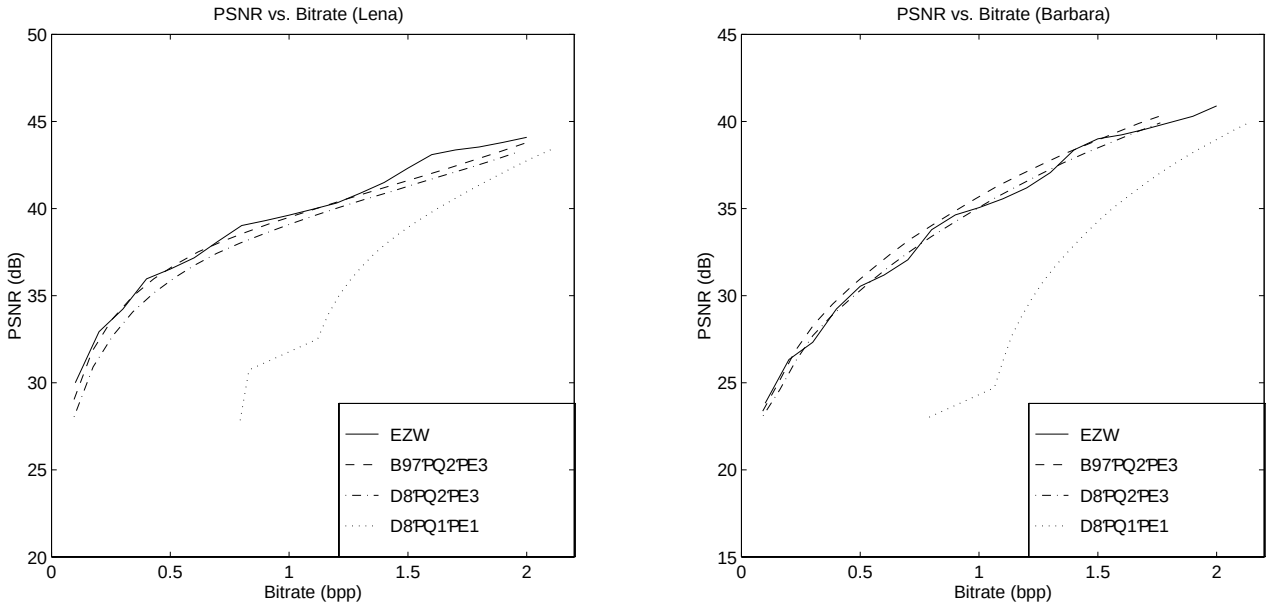

(b)

Figure 6: Comparison of four wavelet image coders. Left and right columns are for "Lena" and "Barbara," respectively: (a) comparison by PQS and (b) comparison by PSNR.

original

B97-Q2-E3 (31.8 dB)

D8-Q2-E3 (30.9 dB)

EZW (32.1 dB)

Figure 7: A visual comparison of "Lena" coded by three wavelet coders at 0.17 bits/pixel. The PQS values are out of valid range and not meaningful in this case.

Table 3: Image quality measured by PQS and PSNR for "Lena."

nominal entropy	B97						D8					
	Q1		Q2		Q3		Q1		Q2		Q3	
	PQS	PSNR	PQS	PSNR	PQS	PSNR	PQS	PSNR	PQS	PSNR	PQS	PSNR
0.1	—	28.875	—	29.042	—	28.910	—	27.849	—	28.039	—	27.952
0.2	0.127	31.823	0.199	31.808	0.270	31.973	—	30.737	0.070	30.908	—	30.843
0.3	1.199	33.622	1.456	33.630	1.490	33.758	0.837	32.517	1.113	32.702	0.958	32.631
0.4	1.988	34.907	2.240	34.949	2.230	35.038	1.645	33.902	1.888	34.064	1.841	34.038
0.5	2.464	35.907	2.756	35.963	2.735	36.054	2.217	35.003	2.453	35.145	2.417	35.128
0.6	2.854	36.744	3.143	36.785	3.126	36.867	2.630	35.875	2.903	36.035	2.869	36.014
0.7	3.152	37.455	3.453	37.512	3.410	37.538	2.951	36.653	3.208	36.742	3.180	36.776
0.8	3.380	38.047	3.684	38.112	3.612	38.116	3.225	37.360	3.486	37.420	3.436	37.430
0.9	3.553	38.583	3.871	38.646	3.806	38.666	3.424	37.954	3.720	38.017	3.644	38.029
1.0	3.692	39.095	4.022	39.156	3.945	39.157	3.606	38.513	3.900	38.567	3.829	38.572
1.1	3.816	39.566	4.150	39.623	4.066	39.648	3.739	39.027	4.066	39.095	3.970	39.082
1.2	3.950	40.050	4.256	40.087	4.173	40.114	3.875	39.514	4.202	39.593	4.105	39.589
1.3	4.043	40.516	4.350	40.539	4.258	40.568	3.999	40.008	4.308	40.061	4.205	40.067
1.4	4.145	40.989	4.428	40.984	4.336	41.015	4.099	40.475	4.403	40.523	4.276	40.547
1.5	4.217	41.454	4.490	41.433	4.398	41.449	4.187	40.956	4.476	40.978	4.345	40.998
1.6	4.276	41.915	4.548	41.863	4.455	41.898	4.270	41.439	4.547	41.433	4.400	41.450
1.7	4.320	42.377	4.600	42.310	4.504	42.342	4.332	41.910	4.608	41.882	4.446	41.913
1.8	4.371	42.866	4.633	42.784	4.551	42.804	4.395	42.405	4.661	42.339	4.496	42.353
1.9	4.412	43.349	4.652	43.263	4.580	43.266	4.451	42.894	4.696	42.797	4.553	42.815
2.0	4.447	43.822	4.668	43.742	4.611	43.737	4.506	43.381	4.718	43.289	4.601	43.288

Table 4: Image quality measured by PQS and PSNR for "Barbara."

nominal entropy	B97						D8					
	Q1		Q2		Q3		Q1		Q2		Q3	
	PQS	PSNR	PQS	PSNR	PQS	PSNR	PQS	PSNR	PQS	PSNR	PQS	PSNR
0.1	0.604	23.228	0.567	23.372	0.751	23.104	0.764	23.023	0.370	23.102	1.139	22.819
0.2	0.941	25.206	0.852	25.062	0.911	25.029	0.957	24.718	0.630	24.599	1.227	24.591
0.3	1.230	26.912	1.300	26.823	1.171	26.776	1.287	26.302	1.185	26.272	1.457	26.191
0.4	1.616	28.397	1.803	28.362	1.552	28.257	1.544	27.662	1.617	27.703	1.705	27.605
0.5	1.935	29.524	2.177	29.519	1.869	29.492	1.859	28.793	2.049	28.852	1.957	28.794
0.6	2.226	30.602	2.517	30.574	2.200	30.500	2.135	29.852	2.310	29.832	2.225	29.762
0.7	2.452	31.556	2.761	31.500	2.499	31.439	2.345	30.842	2.570	30.842	2.416	30.675
0.8	2.651	32.472	2.993	32.416	2.687	32.269	2.562	31.785	2.821	31.711	2.605	31.560
0.9	2.852	33.367	3.205	33.279	2.863	33.080	2.768	32.650	3.026	32.539	2.777	32.445
1.0	3.025	34.198	3.394	34.064	3.020	33.882	2.933	33.486	3.197	33.375	2.941	33.278
1.1	3.173	34.969	3.555	34.833	3.188	34.656	3.080	34.262	3.371	34.151	3.089	34.057
1.2	3.323	35.694	3.703	35.558	3.311	35.383	3.247	35.012	3.520	34.907	3.221	34.792
1.3	3.457	36.398	3.821	36.282	3.469	36.091	3.380	35.692	3.650	35.602	3.354	35.484
1.4	3.572	37.067	3.915	36.940	3.573	36.743	3.505	36.400	3.761	36.282	3.431	36.147
1.5	3.655	37.704	4.026	37.575	3.654	37.358	3.609	37.071	3.855	36.971	3.516	36.769
1.6	3.744	38.315	4.102	38.181	3.728	37.943	3.688	37.721	3.963	37.605	3.595	37.390
1.7	3.815	38.896	4.174	38.767	3.802	38.509	3.777	38.318	4.043	38.219	3.665	37.989
1.8	3.881	39.454	4.220	39.339	3.858	39.089	3.828	38.888	4.126	38.809	3.748	38.589
1.9	3.933	39.986	4.269	39.893	3.903	39.632	3.887	39.465	4.163	39.377	3.801	39.159
2.0	3.992	40.518	4.299	40.416	3.944	40.178	3.935	40.003	4.184	39.922	3.837	39.721

Table 5: Bit rates from E1 for "Lena."

nominal entropy	B97			D8			average bit rate
	Q1	Q2	Q3	Q1	Q2	Q3	
0.1	0.794	0.546	0.547	0.544	0.297	0.297	0.504
0.2	0.831	0.836	0.837	1.080	0.834	0.836	0.876
0.3	1.120	0.882	0.882	1.119	0.877	0.882	0.960
0.4	1.164	1.182	1.181	1.163	1.177	1.179	1.174
0.5	1.210	1.233	1.231	1.206	1.227	1.229	1.223
0.6	1.256	1.285	1.280	1.254	1.278	1.279	1.272
0.7	1.305	1.334	1.332	1.300	1.331	1.328	1.322
0.8	1.355	1.389	1.385	1.349	1.384	1.381	1.374
0.9	1.406	1.444	1.442	1.398	1.439	1.435	1.427
1.0	1.458	1.503	1.499	1.448	1.495	1.489	1.482
1.1	1.511	1.562	1.557	1.500	1.551	1.547	1.538
1.2	1.567	1.621	1.616	1.555	1.609	1.603	1.595
1.3	1.625	1.681	1.677	1.612	1.668	1.662	1.654
1.4	1.685	1.743	1.740	1.672	1.729	1.723	1.715
1.5	1.748	1.805	1.802	1.734	1.791	1.785	1.777
1.6	1.813	1.869	1.866	1.797	1.854	1.849	1.841
1.7	1.879	1.935	1.934	1.865	1.921	1.916	1.908
1.8	1.949	2.006	2.004	1.936	1.988	1.987	1.978
1.9	2.023	2.075	2.078	2.012	2.057	2.060	2.051
2.0	2.102	2.146	2.154	2.091	2.131	2.138	2.127

Table 6: Bit rates from E1 for "Barbara."

nominal entropy	B97			D8			average bit rate
	Q1	Q2	Q3	Q1	Q2	Q3	
0.1	0.791	0.792	0.537	0.788	0.542	0.534	0.664
0.2	1.065	0.819	0.818	0.812	0.817	0.816	0.858
0.3	1.102	1.107	1.101	1.102	1.107	0.851	1.062
0.4	1.136	1.149	1.145	1.141	1.150	0.894	1.102
0.5	1.179	1.193	1.191	1.180	1.195	1.194	1.189
0.6	1.223	1.241	1.241	1.226	1.246	1.249	1.238
0.7	1.272	1.297	1.296	1.274	1.297	1.305	1.290
0.8	1.326	1.354	1.349	1.333	1.358	1.358	1.346
0.9	1.383	1.412	1.408	1.389	1.418	1.414	1.404
1.0	1.442	1.473	1.469	1.445	1.478	1.478	1.464
1.1	1.500	1.535	1.531	1.504	1.540	1.542	1.525
1.2	1.562	1.599	1.594	1.566	1.604	1.608	1.589
1.3	1.626	1.664	1.661	1.632	1.671	1.676	1.655
1.4	1.695	1.732	1.730	1.699	1.738	1.743	1.723
1.5	1.766	1.805	1.800	1.769	1.809	1.813	1.794
1.6	1.839	1.877	1.874	1.841	1.881	1.885	1.866
1.7	1.912	1.954	1.948	1.913	1.955	1.961	1.940
1.8	1.989	2.030	2.026	1.988	2.030	2.038	2.017
1.9	2.067	2.106	2.104	2.065	2.105	2.117	2.094
2.0	2.146	2.184	2.186	2.143	2.184	2.198	2.174

Table 7: Bit rates from E2 for "Lena."

nominal entropy	B97			D8			average bit rate
	Q1	Q2	Q3	Q1	Q2	Q3	
0.1	0.100	0.105	0.097	0.100	0.105	0.097	0.101
0.2	0.193	0.194	0.191	0.195	0.190	0.193	0.193
0.3	0.278	0.284	0.279	0.284	0.279	0.283	0.281
0.4	0.368	0.375	0.368	0.374	0.374	0.372	0.372
0.5	0.457	0.466	0.457	0.464	0.466	0.464	0.462
0.6	0.545	0.557	0.546	0.557	0.560	0.558	0.554
0.7	0.637	0.642	0.639	0.650	0.655	0.653	0.646
0.8	0.731	0.736	0.734	0.750	0.755	0.753	0.743
0.9	0.827	0.834	0.834	0.851	0.856	0.857	0.843
1.0	0.928	0.935	0.936	0.953	0.960	0.960	0.945
1.1	1.030	1.038	1.041	1.058	1.064	1.067	1.049
1.2	1.132	1.142	1.145	1.165	1.170	1.170	1.154
1.3	1.240	1.247	1.249	1.271	1.274	1.275	1.259
1.4	1.348	1.354	1.357	1.379	1.381	1.381	1.367
1.5	1.456	1.461	1.463	1.484	1.487	1.488	1.473
1.6	1.564	1.567	1.570	1.589	1.591	1.593	1.579
1.7	1.672	1.674	1.678	1.696	1.698	1.698	1.686
1.8	1.779	1.784	1.784	1.801	1.802	1.805	1.792
1.9	1.887	1.891	1.891	1.906	1.906	1.906	1.898
2.0	1.994	1.995	1.998	2.008	2.008	2.011	2.002

Table 8: Bit rates from E2 for "Barbara."

nominal entropy	B97			D8			average bit rate
	Q1	Q2	Q3	Q1	Q2	Q3	
0.1	0.099	0.100	0.089	0.094	0.102	0.088	0.096
0.2	0.178	0.185	0.171	0.178	0.185	0.172	0.178
0.3	0.262	0.266	0.251	0.264	0.268	0.252	0.260
0.4	0.341	0.345	0.332	0.346	0.349	0.331	0.341
0.5	0.423	0.428	0.417	0.422	0.429	0.416	0.423
0.6	0.503	0.510	0.504	0.504	0.515	0.505	0.507
0.7	0.584	0.600	0.592	0.585	0.598	0.593	0.592
0.8	0.670	0.687	0.675	0.674	0.691	0.679	0.679
0.9	0.757	0.774	0.760	0.762	0.780	0.763	0.766
1.0	0.847	0.865	0.849	0.847	0.867	0.854	0.855
1.1	0.930	0.953	0.937	0.938	0.958	0.947	0.944
1.2	1.022	1.043	1.028	1.029	1.049	1.042	1.035
1.3	1.112	1.133	1.122	1.123	1.141	1.138	1.128
1.4	1.208	1.225	1.221	1.218	1.234	1.235	1.223
1.5	1.302	1.320	1.318	1.314	1.330	1.333	1.320
1.6	1.401	1.414	1.417	1.414	1.426	1.432	1.418
1.7	1.500	1.514	1.517	1.513	1.525	1.534	1.517
1.8	1.605	1.615	1.620	1.618	1.625	1.638	1.620
1.9	1.710	1.717	1.721	1.722	1.728	1.740	1.723
2.0	1.816	1.819	1.827	1.828	1.835	1.846	1.828

Table 9: Bit rates from E3 for "Lena."

nominal entropy	B97			D8			average bit rate
	Q1	Q2	Q3	Q1	Q2	Q3	
0.1	0.089	0.095	0.089	0.090	0.095	0.090	0.091
0.2	0.169	0.175	0.171	0.170	0.171	0.173	0.172
0.3	0.247	0.258	0.253	0.252	0.254	0.256	0.253
0.4	0.329	0.342	0.335	0.334	0.341	0.340	0.337
0.5	0.413	0.429	0.422	0.419	0.430	0.429	0.424
0.6	0.497	0.518	0.509	0.508	0.521	0.520	0.512
0.7	0.586	0.601	0.600	0.602	0.617	0.616	0.604
0.8	0.680	0.694	0.692	0.703	0.718	0.716	0.700
0.9	0.776	0.793	0.794	0.804	0.818	0.817	0.801
1.0	0.879	0.896	0.896	0.909	0.922	0.922	0.904
1.1	0.983	1.002	1.002	1.012	1.028	1.030	1.009
1.2	1.086	1.106	1.105	1.119	1.134	1.134	1.114
1.3	1.194	1.210	1.213	1.226	1.240	1.240	1.220
1.4	1.303	1.317	1.321	1.336	1.348	1.345	1.328
1.5	1.414	1.430	1.430	1.445	1.457	1.454	1.438
1.6	1.524	1.537	1.538	1.551	1.561	1.561	1.545
1.7	1.634	1.645	1.647	1.659	1.669	1.670	1.654
1.8	1.745	1.757	1.754	1.769	1.777	1.778	1.763
1.9	1.856	1.865	1.866	1.879	1.886	1.884	1.873
2.0	1.966	1.971	1.972	1.988	1.990	1.994	1.980

Table 10: Bit rates from E3 for "Barbara."

nominal entropy	B97			D8			average bit rate
	Q1	Q2	Q3	Q1	Q2	Q3	
0.1	0.088	0.091	0.078	0.082	0.090	0.075	0.084
0.2	0.155	0.162	0.145	0.152	0.158	0.140	0.152
0.3	0.221	0.229	0.214	0.221	0.226	0.212	0.221
0.4	0.291	0.300	0.292	0.297	0.306	0.290	0.296
0.5	0.367	0.379	0.373	0.371	0.384	0.373	0.375
0.6	0.443	0.460	0.453	0.449	0.466	0.454	0.454
0.7	0.521	0.546	0.534	0.525	0.547	0.543	0.536
0.8	0.601	0.626	0.617	0.604	0.629	0.625	0.617
0.9	0.685	0.709	0.699	0.693	0.715	0.705	0.701
1.0	0.777	0.797	0.782	0.782	0.804	0.790	0.789
1.1	0.865	0.889	0.871	0.874	0.896	0.883	0.880
1.2	0.956	0.980	0.961	0.961	0.985	0.973	0.969
1.3	1.043	1.067	1.054	1.054	1.077	1.074	1.062
1.4	1.137	1.160	1.158	1.153	1.173	1.172	1.159
1.5	1.233	1.258	1.251	1.245	1.270	1.272	1.255
1.6	1.330	1.352	1.354	1.346	1.366	1.371	1.353
1.7	1.433	1.452	1.450	1.452	1.470	1.481	1.456
1.8	1.541	1.558	1.562	1.555	1.572	1.579	1.561
1.9	1.641	1.659	1.660	1.661	1.673	1.688	1.664
2.0	1.749	1.763	1.772	1.770	1.784	1.795	1.772